Conclusions: MT was not superior to NB in diagnostic accuracy in benign and atypical papillary lesions. Benign papillary lesions diagnosed by MT or NB might not require immediate excision, but should receive imaging FU. Excisions should be performed in cases showing changes in imaging features, as there was a 5% upgrade rate at excision.

355 Mitochoncdrial DNA Damage Triggers Tumor Progression and Metastasis in PyMT Mice

L Yuzefovych, AG Kahn, GL Wilson, L Rachek. College of Medicine, University of South Alabama, Mobile, AL; University of South Alabama, Mobile, AL.

Background: Breast cancer is the leading cause of cancer death among women worldwide. On a molecular level, it is unclear which of the changes in breast tumors are likely to lead to invasion and metastasis. Among the potential targets are mitochondria, generation of mitochondrial reactive oxigen species (ROS) and mitochondrial DNA (mtDNA). The objective of this study is to determine the involvement of mtDNA damage in breast cancer progression and if the targeting of the DNA repair enzyme hOGG1 into mitochondria prevents tumor progression in a genetic model of breast cancer.

Design: Four groups of female double transgenic mice were generated in our laboratory. We have used the F1 cross of a well-characeterized preclinical transgenic model of metastatic breast cancer male mice (PyMT) with females: 1) Tg, overexpressing a human mitochondrial repair enzyme (hOGG1) in addtion to their endogenous one (OGG1) (n=13); 2) KO/Tg, knockout mice lacking endogenous OGG1 and overexpressing hOGG1 (n=10); 3) KO, knockout mice lacking endogenous OGG1 (n=21); 4) WT, wild type with endogenous OGG1 (n=14). Starting at 16 weeks mice were sacrified and all mammary tumors and lungs removed. The tissue was fixed in formalin, paraffin embedded, and stained with hematoxylin-eosin. The breast neoplasms were classified according to the Annapolis consensus. The number of lung metastastatic foci was recorded. Statistical analysis was performed using ANOVA.

Results: The results are summarized in Table 1.

Table 1

PyMT Mice Genotype	Primary Tumor Incidence	Metastatic Incidence	Average Number of Metastatic Lung Foci
KO	100%	82% *	13.29 ± 2.75
WT	100%	62.5%	11.27 ± 2.04
Tg	100%	33.3% *	0.66 ± 0.15 *
KO/Tg	71% *	36.4% *	1.27 ± 0.3 *

* p≤ 0.05 vs WT group, one way ANOVA

All the neoplasms were advanced invasive carcinomas. A two fold difference in the metastatic incidence in the lungs was noted between the PyMT/Tg and PyMT/WT mice. Lungs from the PyMT/Tg mice had about a 15 fold decrease in the average number of metastatic foci compared to PyMT/WT mice. These differences were statistically significant (p≤0.05).

Conclusions: Based on these data we conclude that mtDNA damage appears to play a role in both progression and the proliferation of distant metastatic foci. These results have potential clinical and translational significance as most current therapies increase oxidative stress, therefore inducing more damage to mtDNA, increase ROS and thus could drive tumor metastasis.

Cardiovascular Pathology

356 Gross Examination of the Left Ventricular Assist Device: A Primer for the Pathology Resident

V Ananthanarayanan, MK Mirza, MB Alikhan, AS Akki, AN Husain. University of Chicago, Chicago, IL.

Background: The advent of left ventricular assist device (LVAD) placement has significantly reduced mortality in patients with cardiac disease. As this translates into an increased incidence of LVAD associated autopsies and explanted hearts, the pathology resident needs an insight into the structural and mechanical aspects of this device as well as its contribution to morbidity and mortality of the patient. Current literature does not elucidate algorithms towards LVAD examination at autopsies. We address the dearth of this information by providing a summary of our experience with LVAD-associated autopsies and present a guide to the examination of these specimens.

Design: Nineteen consecutive LVAD-associated autopsies were included in this study. We tabulated clinical information and carefully examined segments of the device, noted intactness of anastomoses, presence of pre-mortem thrombi, significant hemorrhage and evidence of infection. The heart was dissected as shown in figure 1. Step 1: gross examination of LVAD-aortic anastomosis and LVAD-apex anastomosis. 2. Inspection for thrombi in ventriculo-aortic connection. 3. Analysis of coronary arteries. 4. Dissection along ventral axis to apex. 5 Breadloafing of tissue from apex to base. 6. Removal of LVAD parts for internal inspection. 7. Sampling for histologic examination as appropriate.

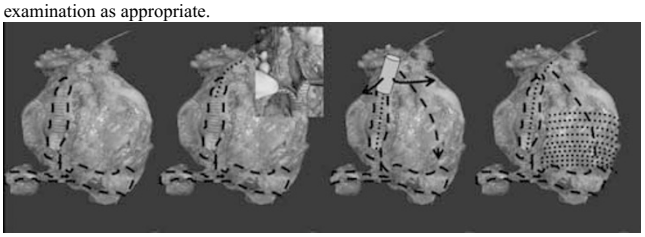

Results: In all 19 cases (100%) suture lines were intact and no defective LVAD was identified. Clinically significant LVAD thrombi were noted in 2/19 cases (10%), significant hemothorax in 1/9 (5%) and 1 case revealed encroachment of the endomyocardium over the LVAD inflow at cardiac apex, leading to functional obstruction (795 days post LVAD).

Conclusions: Correct examination of the LVAD associated cardiac specimen is a crucial component of the medical autopsy. Our dissection approach provides a useful tool in effectively analyzing all potential parts of the device as well as evaluation of the native heart by gross and histologic techniques. In our experience, there was no case of anastomotic leak or death due to a functionally defective LVAD. Although LVAD placement is generally considered a 'bridge' to cardiac transplant, long standing devices may be susceptible to endomyocardial encroachment and functional obstruction.

357 Lipomatous Lesions of the Heart: A Comparative Morphologic and Cytogenetic Study with New Pathogenetic Insights

MC Bois, AM Oliveira, CW Roth, BR Evers, RN Wehrs, JJ Maleszewski. Mayo Clinic, Rochester, MN.

Background: Benign lipomatous lesions of the heart encompass an etiologically diverse group of entities, including neoplastic, congenital, and reparative phenomena. Among these, lipomas and lipomatous hypertrophy of the atrial septum (LHAS) represent two commonly encountered, both presenting as masses. While cardiac lipomas are believed to be neoplastic, there is little supporting genetic evidence. LHAS is thought to represent embryologically entrapped fat that increases in size proportional to visceral adiposity, though supporting genetic data is absent here as well. To date, no study has systematically and comparatively evaluated the morphologic and genetic characteristics of these lesions.

Design: Tissue registry archives of Mayo Clinic were queried for cases of cardiac lipoma and LHAS (1994-2011). Three cases of ventricular fatty infiltration were identified from age-matched autopsy subjects for controls. Clinical, imaging and pathological findings were reviewed. Representative cases in each cohort were evaluated by fluorescence in situ hybridization (FISH) for *HMGA1* and *HMGA2* loci rearrangement via break-apart probes and for *CPM*/*MDM2* locus amplification via enumeration probes.

Results: Four cases of cardiac lipoma were identified (mean age 59 yrs, range 48-64; 2 men); 2 right atrial, 1 left ventricular and 1 pericardial. 42 cases of LHAS were identified (mean age 75.6 yrs, range 45-95, 20 men), 39 of which were autopsy-derived. The majority of these lesions were identified incidentally on imaging or at the time of surgery/autopsy (lipomas, 3; LHAS, 40). The median size was 6.1 cm for lipomas, and 2.8 cm for LHAS (n=14). A single case each of a cardiac lipoma and LHAS were found to harbor *HMGA2* rearrangement, while no case showed molecular cytogenetic abnormality of *HMGA1* or *CPM*. No cases of fatty infiltration exhibited the evaluated cytogenetic rearrangements.

Conclusions: This represents the largest series of histopathologically confirmed cardiac lipomas from a single institution. Additionally, it is the first to evaluate cardiac lipomas for genetic alterations associated with extracardiac lipomoutous lesions. The genetic and morphologic similarities found provide evidence in support of both the neoplastic nature of cardiac lipomas as well as highlighting etiologic similarities in these tumors. This is also the first study to evaluate LHAS and fatty infiltration for cytogenetic alterations. Interestingly and unexpectedly, a single case of LHAS contained an HMGA2 rearrangement, challenging the currently accepted hypothesis of pathogenesis for this lesion.

358 An Evaluation of the Utility of Post-Mortem Computed Tomography in the Diagnosis of Lethal Coronary Artery Atherosclerosis and Hypertensive Heart Disease

CR Curry, VS Snyder, SW Andrews, SL Lathrop, EW Matshes. University of Chicago and NorthShore University HealthSystem, Evanston, IL; University of New Mexico and the Office of the Medical Investigator, Albuquerque, NM.

Background: Autopsy is regarded as the gold standard for the diagnosis of natural disease and trauma in the postmortem setting. Despite this, some centers routinely use postmortem computed tomography (PMCT) scans. Amongst the most common causes of death in any medical examiner jurisdiction are atherosclerotic cardiovascular disease (ASCVD) and/or hypertensive cardiovascular disease (HSCVD). Data does not exist to support or refute the premise that routine use of PMCT is useful for the detection of hypertensive and atherosclerotic cardiovascular disease (HASCVD). Practical experience shows that non-contrast PMCT does not accurately document or diagnose lethal coronary artery atherosclerosis (CAA) and sequelae, nor does it allow for the diagnosis of hypertensive cardiovascular disease.

Design: One hundred adult forensic autopsies were selected from an 18-month period (July 2011 to January 2013). The cases were divided into two age- and sex-matched groups by cause of death: (1) those due to HASCVD, and (2) those due to other causes. Two forensic pathologists, blinded to the cause of death, reviewed pre-autopsy PMCT scans of the chest and recorded the presence or absence of severe coronary artery stenosis (defined as > 75% stenosis), myocardial pathology (including left ventricular hypertrophy and myocardial infarction), cardiomegaly, and coronary artery calcium deposition. The same set of data was obtained from the corresponding autopsy reports. Results of the PMCT interpretations were compared with the results obtained from autopsy.

Results: PMCT did not detect clinically significant CAA and completely missed it in 56 cases where it was proven at autopsy. PMCT did not detect myocardial pathology in 50 cases where it was proven at autopsy and mistakenly detected it in 5 cases where it was not identified at autopsy. PMCT did not detect cardiomegaly in 44 cases where it was identified at autopsy and mistakenly detected it in 5 cases where it was not identified at autopsy. Coronary artery calcium deposition was not identified at autopsy in 46 cases where it was detected by PMCT.

Conclusions: The routine use of PMCT is costly and does not allow for the accurate diagnosis of HASCVD, one of the most common causes of death. Autopsy is the gold standard for detecting HASCVD and sequelae, with the exception of coronary artery calcium deposition, which is clinically insignificant.

359 The ISHLT Antibody-Mediated Rejection Pathologic Grading System for Cardiac Transplantation: How Well Does It Perform?

SA Dean, R Frank, M Kamoun, P Lal. Hospital of the University of Pennsylvania, Philadelphia, PA.

Background: Antibody-mediated rejection (AMR) has proven to be a diagnostic and therapeutic challenge in heart transplantation. The International Society for Heart and Lung Transplant (ISHLT) proposed a new grading system for pathologic AMR (pAMR) in 2011 that combines both histopathologic and immunopathologic features.

Design: In this retrospective, single institutional analysis (2005-2011), we evaluated endomyocardial biopsies (EMBs) from cardiac transplant patients who had concurrent C4d immunofluorescence (IF) and donor specific antibody (DSA) measurements. Each EMB was evaluated by 3 of the authors for the histopathologic features described by the ISHLT (endothelial activation, intravascular macrophages, capillary destruction, edema, neutrophilic infiltrates, capillary fragmentation, hemorrhage, and endothelial cell pyknosis). EMBs were then categorized according to the new ISHLT pAMR grading system. C4d IF was considered positive only if >50% interstitial capillary staining was observed.

Results: The classification of 106 EMBs evaluated with the new pAMR grading system is shown in the table below. Circulating DSA was observed in 48% (51/106) of patients spanning across all grades (AMR0 to AMR3). Of the 86 patients classified as AMR0 and AMR1-h, DSA positivity was found in 38% (33 cases). In addition, we observed that not all individual histologic features associated with pAMR independently correlated with the DSA status of patients. However, when we analyzed the data taking all histologic features into consideration, the new ISHLT 2011 pAMR grading system correlated well ($p < 0.01$) with the presence of DSA.

ISHLT 2011 pAMR Grade	Number of Biopsies	Number Positive for DSA	Number Positive for IF
AMR0	38	12	0
AMR1-h	48	21	0
AMR1-i	3	2	3
AMR2	13	13	13
AMR3	4	3	1
	106	51	17

Conclusions: The ISHLT 2011 pAMR grading system appears to have a statistically significant correlation with DSA. Patients with AMR1-h are considered suspicious for pathologic AMR and by definition are negative for C4d. In our cohort, 44% of AMR1-h patients showed evidence of DSA. This finding identifies a subset of patients that may benefit from further investigation into their clinical presentation and long term outcomes.

360 Antibody-Mediated Rejection in Endomyocardial Biopsies as Assessed by Automated C4d and CD34 Quantitation and Co-Localization

R Frank, T Baradet, MD Feldman, P Lal. Hospital of the University of Pennsylvania, Philadelphia, PA.

Background: Antibody-mediated rejection is clinically significant and predisposes patients to severe graft dysfunction and graft loss. Detection of AMR in cardiac transplant patients relies, in part, on the immunofluorescence (IF) pattern of C4d. Often only one endomyocardial biopsy (EMB) is obtained for rejection assessment. IF labeling is not used for formalin-fixed paraffin-embedded (FFPE) tissue because of autofluorescence. Spectral imaging can overcome autofluorescence interference, allowing FFPE sections for C4d evaluation via imaging.

Design: A retrospective cohort (2005-2011) of EMB with concurrent C4d IF and anti-HLA donor specific antibodies (DSA) were sectioned and stained for CD34 and C4d. DSA were evaluated against HLA class I and class II specificities pre and post transplant using flow cytometry and/or Luminex bead assays. IF images of the sections were acquired using a spectral imaging system and analyzed using an automated morphologic image analysis software package to assess C4d staining in capillaries. The software automatically identifies capillaries with CD34 and measures the C4d in capillary walls and the area immediately surrounding the capillaries. Automated measures were compared to visual assessments.

Results: Autofluorescence-free IF images from 26 FFPE specimens were obtained using spectral imaging. Of the 26 EMB, IF on frozen tissue revealed that 12, 7, and 7 were positive, negative or had <50% staining for C4d. C4d intensity of 1+, 2+ and 3+ were found in 5, 8, and 4 EMB with 2 EMB having variable staining. DSA was present in 23 patients while 3 were negative. Automated morphologic analysis of the images identified vessels and quantified the C4d intensities within those regions. Results from FFPE specimens were comparable to those from frozen, and the image-based objective measure of rejection status gave good correlation to visual assessment. As the percentage (0, 1-49 and >50) and intensity (0-1+, 2+, 3+) of C4d increased on the frozen IF EMB tissue, the quantitation of C4d on FFPE for percentage (0.24, 0.45 and 0.65) and intensity (0.45, 0.52 and 0.81) also increased.

Conclusions: Automated quantitation of dual-labeled (CD34 and C4d) and co-localized FFPE EMB specimens can be achieved using spectral imaging and morphologic image analysis software which supports the frozen tissue IF visual assessment. Spectral imaging and analysis has the potential to aid in the clinical assessment of cardiac transplant biopsies.

361 FFPE-TMA MALDI Mass Spectrometry Reveals Altered Protein Expression in Sudden Cardiac Death Hearts

MK Halushka, EH Seeley, RM Caprioli, JJ Maleszewski, R Virmani, DE Arking. Johns Hopkins University SOM, Baltimore, MD; Vanderbilt University, Nashville, TN; Mayo Clinic, Rochester, MN; CVPath, Inc, Gaithersburg, MD.

Background: Sudden cardiac death (SCD) is a major cause of death worldwide. Recent genetic studies have identified specific genes associated with the SCD phenotype. Tools to perform global proteomic studies in SCD have not existed until now. We sought to determine proteomic alterations in SCD using matrix-assisted laser desorption/ionization (MALDI) imaging mass spectrometry (IMS) on cardiac tissue microarrays (TMAs).

Design: We created two TMAs containing left ventricle free wall cores from SCD cases and matched controls from the autopsy files of CVPath, Johns Hopkins, and Mayo Clinic. The CVPath TMA contained 340 0.4mm tissue cores (184 SCD cases, 91 non-SCD controls and additional control tissues). The Mayo Clinic TMA contained 208 1 mm tissue cores containing 100 SCD cases and 100 non-SCD controls. Ten micron sections were cut from each TMA block onto an indium tin oxide-coated slide. Six to thirty-two peptide mass spectra were obtained from each core using a Bruker AutoFlex Speed mass spectrometer in positive ion reflection mode.

Results: In the TMAs, 873 spectral peaks were identified. General linear mixed models, used to account for repeated sample measurements, along with principal components analysis to correct for technical artifacts, were used to identify spectral peaks associated with SCD status. Five peaks were significant in both arrays ($P<0.005$ in each array) with the same direction of effect, with the most significant peak at 862.75 ($P=3.2\times10^{-4}$, $P=8.5\times10^{-5}$). The specific proteins corresponding to these peaks remain to be identified.

Conclusions: We have used novel proteomic methods to begin to unravel cardiac alterations in sudden cardiac death. These agnostic, high-throughput evaluation methods are certain to yield new clinical insights into this devastating disease.

362 Pathology of Chronic Chagas Cardiomyopathy in the United States: A Detailed Review of 12 Cardiectomy Cases

EP Kransdorf, MC Fishbein, LSC Czer, JK Patel, A Velleca, JA Kobashigawa, DJ Luthringer. Cedars-Sinai Heart Institute, LA, CA; University of California Los Angeles, LA, CA; Cedars-Sinai Medical Center, LA, CA.

Background: Chagas disease (CD) is endemic in Central and South America, the result of infection with the parasite Trypanosoma cruzi (TC). Chronic infection leads to Chagas cardiomyopathy (CC), treatment of which can include heart transplantation (HT). Due to the rarity of CD in the United States (US), very few transplantations for CC occur, and thus the pathologic features are not widely appreciated and diagnosis can be complicated. With increasing population diversity in the US, higher frequencies of CD are occurring. The purpose of this study was to conduct a detailed analysis of the gross and microscopic features of CC cardiectomy specimens from patients undergoing HT in the US, to better understand the pathology and improve the recognition of CC.

Design: A retrospective review of HT patients and total artificial heart (TAH) recipients from Cedars-Sinai and UCLA Medical Centers (2006-2013) was undertaken. Cardiectomy specimens from patients with positive serology for TC were evaluated. Gross features assessed included weight, ventricular dilatation, patterns of scarring, epicardial plaque, aneurysm characteristics and mural thrombi. Histologic features assessed and graded included presence of TC; degrees (0=none;1=focal;2=multifocal) of fibrosis, necrosis, myocytolysis; presence of vasculitis & granulomas; degrees & location of cell infiltration, specifically plasma cells, lymphocytes, eosinophils, histiocytes, neutrophils & giant cells.

Results: From over 400 HT and TAH patients, 12 CC cases were identified (cohort profile: 11 HT, 1 TAH; 5 male, 7 female; age at HT 37-69 years; all natives of CD endemic countries). All hearts showed dilated cardiomyopathy (mean heart wt 389 g); 3 had left ventricular apical aneurysms; 5 had epicardial fibrotic plaques and 7 had mural thrombi. 2 cases showed rare intracytoplasmic TC organisms. Microscopic features present in all 12 cases included interstitial fibrosis & myocarditis with lymphocytes, plasma cells & eosinophils; 7 hearts had granulomas, 4 had giant cells.

Conclusions: CC in the US is characterized by ventricular dilatation with mural thrombi and eosinophilic myocarditis. Apical aneurysm, a characteristic feature, and epicardial fibrotic plaques are present in less than half of cases. Histologic clues to the diagnosis are interstitial fibrosis and eosinophil-rich myocarditis. Granulomas do not exclude the diagnosis. Histologic confirmation of TC as the etiologic agent is rare.

363 Morphologic Patterns of Cardiac Amyloid Deposition Correlate with Amyloid Subtype as Confirmed by Mass Spectrometry: A Proteomic and Histologic Analysis of 108 Cases

BT Larsen, WD Edwards, OM Mereuta, S Dasari, DL Murray, PJ Kurtin, JD Theis, JA Vrana, JJ Maleszewski. Mayo Clinic, Rochester, MN.

Background: Accurate subtyping of cardiac amyloidosis is paramount, as prognosis and treatments vary widely by subtype. Mass spectrometry is the gold standard, but is not widely available; serum/urine protein electrophoresis (SPEP/UPEP) with immunofixation (IFE) and free light chain (FLC) immunoassays are less sensitive and specific, and immunohistochemistry is unreliable. It is not known whether histologic patterns of deposition are predictive of subtype.

Design: All autopsy cases with cardiac amyloidosis (1998-2010) were retrieved from institutional pathology archives. Subtyping was performed by laser capture microdissection with mass spectrometry-based proteomic analysis. Results of SPEP/UPEP/IFE and FLC studies were recorded. Patterns and extent of interstitial and vascular deposition, assessed by light microscopy, were recorded and analyzed for statistical correlation with protein subtype.

Results: Among 108 decedents (mean age 75 yrs, range 42-101; 69% men), a single subtype was present in 103 cases, including transthyretin receptor (ATTR; 58 cases), immunoglobulin light chain (AL)-λ (30), AL-κ (12), ASAA (2), and AAPOA4 (1). Five cases showed co-deposition with heavy chain (AH, 4 γ, 1 α), including AH/AL-λ (3), AH/ATTR (1), and AH/AL-λ/ATTR (1). SPEP/UPEP/IFE and FLC assays showed variably low sensitivities and specificities for predicting subtype. Observed morphologic patterns included dispersed pericellular, discrete pericellular, nodular, and endocardial interstitial deposition, as well as vascular deposits. When interstitial deposition was present, its severity was strongly associated with subtype (p=0.0002), with greater amyloid burden in AL versus ATTR (odds ratio [OR]=19.0; p=0.0054). Interstitial patterns were often mixed, but dispersed pericellular and endocardial deposits were each more likely to be AL than ATTR (OR= 13.0 and 42.09, p=0.0001 and <0.0001, respectively), nodular deposits were more likely to be ATTR than AL (OR= 3.05, p= 0.0239), and the discrete pericellular pattern tended to favor ATTR over AL (OR=2.13, p=0.0838). Arterial and venous deposits were each more likely to be AL than ATTR (OR= 6.07 and 114.7, p<0.0001 and p<0.0001, respectively).
Conclusions: The extent and distribution of cardiac amyloidosis strongly correlate with subtype, suggesting fundamental subtype-specific differences in the pathobiology of amyloid deposition in the heart. The tendency for mixed patterns to occur indicates that histology is not accurate enough to replace mass spectrometry for subtyping in individual cases.

364 Is There an Intermediate Diagnostic Category between Sarcoidosis and Idiopathic Giant Cell Myocarditis?

JJ Maleszewski, BT Larsen, MC Castonguay, RK Young, LT Cooper, MK Halushka. Mayo Clinic, Rochester, MN; Dalhousie University, Halifax, NS, Canada; The Johns Hopkins Hospital, Baltimore, MD.
Background: A decade has passed since recognition that idiopathic giant cell myocarditis (IGCM) and cardiac sarcoidosis (CS) were distinct clinicopathologic entities. Despite the significant differences in prognosis, occasional cases have histomorphologic overlap between the two diseases making definitive diagnosis and prognostication difficult if not impossible. We investigated a collection of cardiac surgical and autopsy cases to determine if a distinct intermediate entity (INT) could be identified.
Design: Tissue archives from 3 large academic medical centers were searched for cases of IGCM, CS, and granulomatous myocarditis. Three cardiovascular pathologists (blinded to the original diagnosis) semiquantitatively graded the components and characteristics of the inflammatory infiltrate as well as general histopathologic features such as necrosis and fibrosis. Cases were classified as IGCM and CS based on published criteria. Indeterminate cases were indicated as such. Clinical presentation and course were also documented along with relevant imaging and microbiologic data. A Fisher exact test and a Mann Whitney U test were used as appropriate.
Results: Forty-six cases were identified (mean age 55.4 yrs, range 17-76 yrs; 42% women). Complete follow-up was available in 43 patients. Parenchymal necrosis was seen in 14 (67%) cases of IGCM, 5 (45%) INT cases, and no cases of CS ($p=0.$0002 between IGCM and CS). On a 0-3 scale, eosinophilic infiltrate increased from CS (1) to INT (1.25) to IGCM (1.86). On a 0-2 scale, lymphocytic infiltrate was highest in IGCM (1) and lower in INT (0.58) and CS (0.23). A well-circumscribed border to the granuloma was present in 92% of CS cases, 75% of INT cases and 18% of IGCM cases (p=0.0002 between IGCM and CS and p=0.02 between IGCM and INT). Biopsies in the INT category had an intermediate incidence of ventricular tachycardia (43%) vs. IGCM (35%) or CS (77%). Death within a year of histologic diagnosis was seen in 8 (38%) IGCM patients and 1 each for INT (9%) and CS (9%). Mortality at any time point was significantly higher among IGCM patients, 12 (57%) vs. INT 3 (27%) or CS 1 (2%) cases (p=0.02).
Conclusions: A subset of patients with granulomatous myocarditis have a giant cell infiltrate that is difficult to classify into IGCM or CS. Despite histologic findings that can be similar to IGCM, patients in the INT category have survival more similar to CS cases and are likely to have a less aggressive course than IGCM.

365 Beyond Epicardial Arteries: Assessing Coronary Microvascular Remodeling in End-Stage Heart Disease

M Mancini, C Giordano, CRT Di Gioia, C Preziuso, M Orlandi, P Lilla Della Monica, P Gallo, P Camici, G d'Amati. Sapienza University of Rome, Rome, RM, Italy; S. Camillo-Forlanini Hospital, Rome, RM, Italy; Vita-Salute University and San Raffaele Scientific Institute, Milan, MI, Italy.
Background: Coronary microcirculation made up of intramural pre-arterioles and arterioles, plays a crucial role in regulating myocardial blood flow. Structural and functional abnormalities of cardiac microcirculation have been shown in hypertensive heart disease, hypertrophic cardiomyopathy, myocardial storage disease etc. They have been linked to myocardial ischemia, however the exact role of coronary microvascular remodeling (CMR) in the development of end stage heart disease (ESHD) has yet to be fully elucidated.
Design: Our aim was to assess the presence and detail the morphologic features of CMR in ESHD of different etiologies. We examined 45 consecutive end-stage failing hearts from transplant procedures performed in a five-year span (January 2008-May 2013). Pathologic diagnosis was based both on gross and microscopic analysis according to a detailed study protocol.
Results: Our population consisted of 37 males and 8 females (mean age at transplant of 48±12 years). Epicardial coronary artery disease accounted for the majority of cases 23/45 (51%) we found CMR in 12 of these hearts (52%), mostly with a histologic pattern of concentric medial hypertrophy (CMH) and perivascular fibrosis 11/12 (91%). Dilated cardiomyopathy was diagnosed on pathologic grounds in 14/46 cases (30%). We found CMR [both CMH and eccentric medial hypertrophy (EMH)] associated with microscopic scarring in 12/14 (85%) of these hearts. Interestingly, 3 of these cases had a pre-transplant diagnosis of ischemic heart disease, with normal epicardial arteries on angiography. Three hearts had gross and microscopic features of hypertrophic cardiomyopathy, showing diffuse CMR with severe CMH and perivascular fibrosis, always associated with scarring and interstitial fibrosis. One patient had a clinical diagnosis of hypertensive cardiomyopathy and showed CMR with very limited scarring fibrosis. No CMR was found in hearts with congenital heart disease, valvular heart disease or restrictive cardiomyopathy.
Conclusions: According to our results, the overall prevalence of CMR in the hearts we examined was 62%, implying a role of microvascular disease in the natural history of ESHD. Quite of interest is the high prevalence of arteriolar remodeling in patients with dilated cardiomyopathy which is also supported by reduction of coronary flow reserve assessed in vivo by others. These findings suggest that at least a subset of patients could take advantage of targeted therapies aimed to counteract CMR before reaching ESHD.

366 C4d Immunoreactivity in Endomyocardial Biopsies after Heart Transplantation: A 10-Year Prospective Analysis

MK Mirza, S Fedson, AN Husain. University of Chicago, Chicago, IL.
Background: In the past decade C4d has emerged as a potential marker for AMR, however, literature regarding its use as a prognostic tool has been controversial. Currently, the ISHLT recommends C4d staining only in the first 90 days post-transplant. Our aim was to prospectively determine the prognostic value of C4d positivity in post-transplant endomyocardial biopsies (EMBs) by correlating with clinical cardiac dysfunction, cellular rejection, HLA status, death, and cardiac allograft vasculopathy (CAV) at autopsy.
Design: All 5862 endomyocardial surveillance biopsies from 241 consectuvie heart transplant recipients (transplant date 1/2002 – 12/2012) were stained prospectively for C4d from 2004. Immunohistochemical stains were performed on paraffin-embedded tissue using an anti-human C4d polyclonal antibody. Only strong diffuse endothelial staining was considered positive. All patients had at least 1 year of follow-up. Cardiac dysfunction at the time of positive biopsy was evaluated by hemodynamics and echocardiography. Cellular rejection was graded per ISHLT 1990 criteria.
Results: Positive C4d staining was present in 64 biopsies from 34 (14%) patients, 9 of whom (26%) had clinically significant cardiac dysfunction. 22/34 (65%) of C4d positive patients died. Autopsy was performed on 19 (8 C4d negative and 11 C4d positive patients) of the 58 deaths. 11/11 C4d positive patients had histologic evidence of CAV. Six of 8 C4d negative patients (75%) had no CAV, while 2 of 8 did. Time to first episode of C4d positivity was 406±383 (7-1302) days. Time to C4d positivity in 12 surviving patients was 224±191 days and in the 22 expired patients was 505 ± 427 days.
Conclusions: In this study, C4d positive patients were younger (by a decade), had higher PRAs and higher mortality (65% vs. 17%) as compared to C4d negative patients. Later C4d positivity is not benign; warranting long-term surveillance. All 11 C4d positive autopsies revealed CAV as the cause of death. Even 1 episode of C4d positivity correlated with a poorer outcome. These findings show a positive association of C4d with CAV and death. Our results indicate a prognostic role for C4d in heart transplantation warranting routine detection (including long-term surveillance) of this marker in the pathologic evaluation of cardiac AMR.

367 Is Ultrastructural Characterization of Endomyocardial Biopsy Useful?

N Narula, I Sobol, MT Ganger, E Horn, SV Seshan. Weill Cornell Medical College, New York, NY.
Background: The popularity of endomyocardial biopsy (EMB), especially its ultrastructural (US) characterization in unexplained recent onset or worsening heart failure (HF) patients (pts) has significantly decreased. Although its impact on the clinical management of HF has not been systematically evaluated, it has influenced the availability of study material, and potentially understanding the mechanisms of disease. Our institution has continued to perform non-transplant biopsies over several years.
Design: We analyzed our experience of 146 consecutive EMB performed over 18 month period- 2011-2013. US analysis was performed in 47 patients. A piece was fixed for US analysis in selected cases. Biopsies were examined by light microscopy (LM) and by US examination.
Results: There were 23 females and 30 males with a age range of 22 to 89 years. Non-specific changes of myocyte hypertrophy and injury were seen in 27 patients by both LM and US examination. Specific changes on EMB were further classified as infiltrative, toxic/drug induced, genetic & those associated with autoimmune disease. In 8 EMBs diagnosis of amyloid could definitively be made on LM, however, in 2 patients diagnosis was made only after US analysis only. Diagnosis of possible drug (adriamycin in 3 and hydroxychloroquin in 3 pts) toxicity was made after US examination. 1 patient had marked myocyte damage with lipid accumulation by US suggesting metabolic/ toxic CM. 1 patient had focal mitochondrial abnormalities by US that lead to genetic testing and a diagnosis of MELAS syndrome. 2 patient with autoimmune diseases had abnormal microvasculature.
Conclusions: The yield of routine US examination of EMB in HF in our cohort is 24%. However, it contributes to assessment of patients with suspected or unsuspected cardiotoxicity, occasionally allows diagnosis of disorders such as amyloid not forthcoming from LM, and rarely provides diagnosis of unsuspected diseases associated with characteristic US findings. We suggest that a tissue specimen be obtained for US in every case and pursue US examination after LM assessment and after combined assessment of clinical and imaging findings.

368 A Component-by-Component Characterization of Vulnerable Plaques by Multiphoton Microscopy

N Narula, M Jain, B Wu, J Narula, S Mukherjee. Weill Cornell Medical College, New York, NY; Icahn School of Medicine at Mount Sinai, New York, NY.

Background: Atherosclerotic plaques vulnerable to rupture are almost always intensely inflamed, include a large lipid core and are covered by a thin fibrous cap. The other components may include neovascularization, intraplaque hemorrhage, and spotty calcification. On the other hand, stable plaques are often devoid of lipid-rich lesions and are characterized by predominant presence of smooth muscle cells and collagen. The present study is a proof of principle experiment to evaluate the feasibility of multiphoton microscopy (MPM) to identify various plaque components.

Design: MPM is a nonlinear optical technique that allows the imaging of fresh or formalin-fixed tissue based on intrinsic signals, including autofluoresence and higher-order scattering. It can generate histology-quality images without the need for tissue fixation, sectioning or staining. In our study, MPM imaging was performed on morphologically diverse aorta and coronary artery plaques obtained during routine autopsy. Fresh unfixed aorta specimens and formalin-fixed paraffin embedded unstained sections of coronary arteries were examined. Coronary artery sections were deparaffinized before MPM examination.

Results: Various components in a plaque were reliably recognized by MPM as shown in the image Figure 1. Hemorrhage (1A), Cholesterol crystals/clefts (1B), fibroatheromas (1C), spotty calcification (1D), fibrous plaque (1E) as well neovascularization were distinguishable.

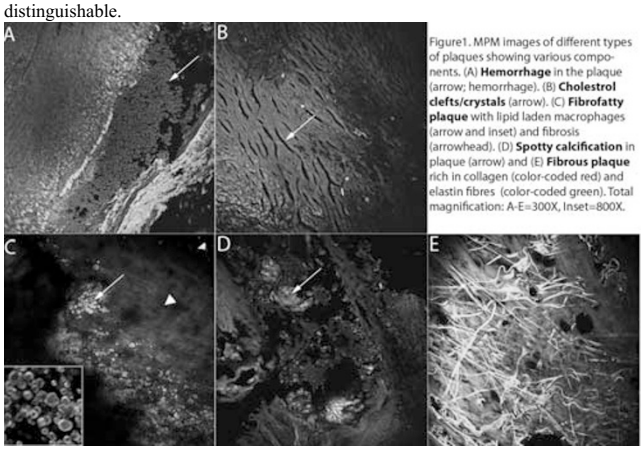

Figure1. MPM images of different types of plaques showing various components. (A) **Hemorrhage** in the plaque (arrow; hemorrhage). (B) **Cholestrol clefts/crystals** (arrow). (C) **Fibrofatty plaque** with lipid laden macrophages (arrow and inset) and fibrosis (arrowhead). (D) **Spotty calcification** in plaque (arrow) and (E) **Fibrous plaque** rich in collagen (color-coded red) and elastin fibres (color-coded green). Total magnification: A-E=300X, Inset=800X.

Conclusions: Recognition of distinct signatures of various plaque components as observed in the present study suggests that MPM has the potential to offer a next-generation characterization of atherosclerotic plaques. It might complement currently available optical coherence tomography (OCT) imaging, which provides a larger field of view and greater imaging depth, whereas MPM has the advantage of significantly higher lateral resolution (comparable to routine histology), allowing greater ease of identification of various tissue substructures. The obvious next step would be the investigation of intact vessels ex-vivo.

369 Anatomical Study of Right Atrial Appendage and Surrounding Structures: Implications for the Atrial Permanent Pacing

S Rizzo, F Zoppo, A Corrado, G Thiene, C Basso. University of Padua, Padua, Italy; Cardiology, Mirano Hospital, Mirano (VE), Italy; Cardiology, Mestre Hospital, Mestre (VE), Italy.

Background: The gross anatomy of the right atrial appendage (RAA), its relationships with the crista terminalis (CT) and the taenia sagittalis (TS) and related clinical implications for atrial permanent pacing have been poorly described. The RAA is the most common region where leads for the permanent atrial pacing are placed. Recently, a rare but life threatening complication, related to the aortic root perforation by a screw-in atrial lead, has been reported. We sought to describe the RAA morphology and relationships with the surrounding cardiac structures, focusing on the regions for atrial leads placement.

Design: An anatomical review of a consecutive series of human hearts specimens coming from routine autopsies is reported. A total of 100 human hearts have been examined to analyze the macroscopic anatomy of RAA, CT and TS; cases with extensive right atrial surgery have been excluded. Attention was paid to the anatomic variability of TS in its "entrance" into the RAA.

Results: The TS has shown 3 main types of anatomic variability related to the presence of a main trunk TS (type 1, present in 76% of cases), double TS (type 2 present in 13% of cases) and a fine arborization without a clear TS representation (type 3 present in 10% of cases). A triple morphology of TS was found in one case. The RAA region proximal to TS routing ("antral RAA region") faces the aortic root, without a clear pericardial space in between; the distal deeper region of the RAA, behind TS ("saccular RAA region") faces even though not closely, the pulmonary artery infundibulum, due to its "unbound" nature that better complies the atrial systolic cycles. This could represent a safer region for leads placement, especially when screw-in leads are used.

Conclusions: The TS morphology is mainly represented as one trunk and, less frequently, two main trunks, connecting anteriorly the CT to RAA. Two separate regions can be identified within the RAA, separated by the TS routing: the "saccular" distal RAA, which could represent a safer region for atrial leads insertion and anchorage, and the "antral" proximal RAA, which is close to the ascending aorta. This may have clinical implications for screw-in atrial leads technologies.

370 Cardiac Allograft Assessment: A Single Institution Experience

S Sayeed, MO Idowu, MM Grimes, CG Uram-Tuculescu. Virginia Commonwealth University Hospital System, Richmond, VA.

Background: Cardiac allograft antibody-mediated rejection (AMR) is recognized as an important form of allograft dysfunction. The 2010 International Society for Heart and Lung Transplantation (ISHLT) consensus conference formulated recommendations regarding the timeline for routine monitoring endomyocardial biopsies for AMR (at 2 weeks, 1 month, 3 months, 6 months, and 1 year, yearly afterwards); handling specific clinical situations in which AMR is suspected; and a new pathologic grading scale based on histologic features and immunopathologic results. The aim of this study was to determine how closely these guidelines are followed in our institution.

Design: A review of all cardiac biopsies with immunofluorescence (IF) studies from 01/2010 to 06/2013 performed at our institution was conducted. In each case the following information was recorded: interval from the date of transplant, clinical rationale for ordering IF , results of IF, histologic findings for AMR, and treatment. We also reviewed the histology of all cases with IF to determine the correlation between histopathologic features of AMR and IF results.

Results: Of the total 566 allograft biopsy, 158 cardiac allograft biopsies with IF studies were identified (28% of all cardiac biopsies). The majority (68%) of cases with positive IF results were identified in biopsies performed >1 year after transplant (figure 1). Abnormal cardiac catheterization findings (45%) were the most common reason for ordering an IF study. 74% of cases with positive IF showed mixed cellular and AMR. There is strong positive correlation between histology and IF results as histopathologic features of AMR were identified in 86% of IF positive cases.

Findings in Cardiac Biopsies with IF Studies

		IF ordered (n= 158)	
		IF positive (n= 19)	IF negative n= 189)
Timeline (from date of transplant)	1 week - 1 month (n=27)	3 (16%)	24 (17%)
	2 - 6 months (n=30)	2 (11%)	28 (20%)
	6 months -1 year (n=14)	1 (5%)	13 (9%)
	>1 year (n=87)	13 (68%)	74 (53%)
Reason for IF	Clinical symptoms (n=26)	6 (25%)	20 (14%)
	Routine/baseline (n=52)	1 (5%)	51 (37%)
	Abnormal cardiac catheterization results (n=72)	11 (58%)	61 (44%)
	Follow Up/Previous positive IF (n=7)	1 (5%)	6 (4%)
	Other (n=1)	0 (0%)	1 (1%)
Biopsy findings	0R (n= 60)	5 (26%)	55 (40%)
	1R (n=82)	8 (42%)	74 (53%)
	2R (n= 13)	5 (26%)	8 (6%)
	3R (n= 3)	1 (5%)	2 (14%)
	AMR positive (by histology) (n=19)	17 (89%)	N/A
Treatment	No change	4 (21%)	106 (76%)
	Immunosuppression and Plasmapheresis	9 (47%)	3 (2%)
	Steroids/Immunosuppression	6 (30%)	26 (19%)
	Other	0 (0%)	4 (3%)

Conclusions: There appears to be variable adherence to the ISHLT guidelines. As patients may have AMR without clinical symptoms, strict adherence to the ISHLT guidelines may identify more patients with subclinical AMR. The strong positive correlation between the histologic features of AMR and IF results suggest that pathologists should evaluate all cardiac allograft biopsies for the histologic features of AMR and report these features as recommended by the ISHLT consensus statement.

371 Utility of Imaging Mass Spectrometry for Detection of Abnormal Myocardial Desmin Deposition – Analysis of Desmin-Related Cardiomyopathy and Other Cardiac Diseases

Y Shintani, T Hayasaka, D Maeda, M Tanaka, M Setou, M Fukayama. The University of Tokyo, Tokyo, Japan; Hamamatsu University School of Medicine, Hamamatus, Shizuoka, Japan; Tokyo Metropolitan Hiroo Hospital, Tokyo, Japan.

Background: Desmin plays a key role in structure and intracellular signaling of myocytes and cardiomyocytes. Both inherited and de novo mutations of desmin and its accessory proteins can lead to desmin-related cardiomyopathy (DRM). DRM is characterized by accumulation of protein aggregates within myocytes leading to hypertrophic cardiomyopathy (HCM), dilated cardiomyopathy (DCM) or restrictive cardiomyopathy. These aggregates, in general, are reported to show positive immunoreactivity for desmin. However, these aggregates are not always stained well on paraffin embedded tissue. Imaging mass spectrometry (IMS) has been recently introduced in the fields of proteomics and metabolomics. This study used IMS on formalin-fixed paraffin-embedded (FFPE) specimens to analyze composition of aggregated protein.

Design: We examined two cases of each of the following: typical DCM, dilated-phase HCM, DRM, and normal controls. The protein component of the tissue sections was directly analyzed using a matrix-assisted laser desorption/ionization (MALDI) time-of-flight (TOF)/TOF-type instrument (ultraflex II TOF/TOF, Bruker Daltonics) after trypsin digestion. Following statistical analysis, MS/MS analysis was performed for the *m/z* signal with a significant difference between DRM and other cases to identify the molecular species using a MALDI-IT-TOF MS (iMScope, Shimadzu).

Results: Many characteristic *m/z* signals were observed in DRM aggregates, which were not found in the DCM, dilated-phase HCM, or normal control tissues. One of these signals, *m/z* 1032, was speculated as desmin with significant homology. The intensity of some *m/z* signals was higher in normal tissues than in the DRM samples. One of these signals, *m/z* 976, was identified as actin with significant homology.

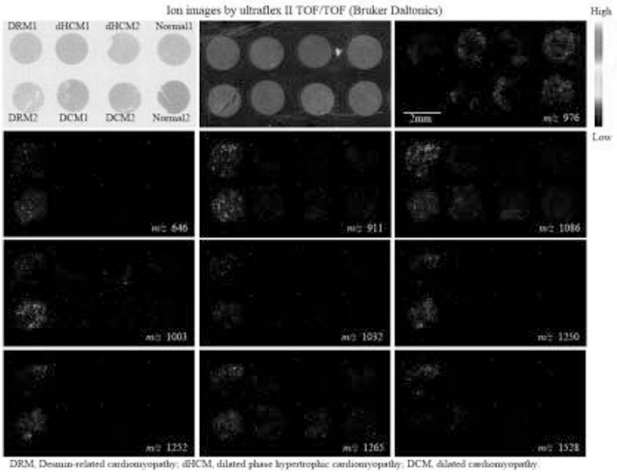

DRM, Desmin-related cardiomyopathy; dHCM, dilated phase hypertrophic cardiomyopathy; DCM, dilated cardiomyopathy.

Conclusions: This is the first study showing that IMS can visualize desmin deposition in the myocardium of DRM patients. IMS can be a useful modality to diagnose DRM even with small FFPE specimens.

372 Morbid Obesity Is Not a Risk Factor for the Development of Clinically Significant Coronary Artery Atherosclerosis

VS Snyder, CR Curry, SL Lathrop, EO Lew, EW Matshes. University of Chicago and NorthShore University HealthSystem, Evanston, IL; University of New Mexico and the Office of the Medical Investigator, Albuquerque, NM; Miami-Dade Medical Examiner Department, Miami, FL.

Background: Obesity has become an epidemic in the United States and has impacted every field of medicine. Patients with morbid obesity [body mass index (BMI) > 40 kg/m^2)] have high rates of sudden unexpected cardiac death, but the mechanism of death is often undetermined. Obesity presents a challenge for pathologists as there is often no acute anatomic cause of death. Cardiovascular complications related to obesity include systemic and pulmonary hypertension, obesity cardiomyopathy, heart failure, left ventricular dilatation and hypertrophy, arrhythmias, and sudden cardiac death. Studies have shown that cardiac related deaths in obese patients often occur in the absence of coronary artery atherosclerosis (CAA). The aim of this study was to determine and compare the prevalence of severe CAA in morbidly obese and normal weight decedents.

Design: Demographic and autopsy data spanning 17 years (1991-2007) was collected from the case files of 53,500 consecutive death investigations performed at a major metropolitan medical examiner department. Study inclusion criteria were: (a) a complete autopsy was performed, (b) the case file was complete and available for review, (c) the body did not have evidence of putrefactive decomposition, embalming, or thermal change, (d) organ/tissue procurement had not taken place, and (e) the heart was atraumatic. The population of morbidly obese (BMI > 40 kg/m^2) decedents (N_{cases} = 1290) was identified, and sex- and age-matched case controls of non-obese (BMI < 25 kg/m^2) decedents ($N_{control}$ = 2572) were selected. Clinically significant CAA was defined as > 75% stenosis.

Results: Both the study and control groups had 59% male and 41% female decedents. The average age for both groups was 47 years. The mean BMI for study cases was 46.5 kg/m^2. The mean BMI for the control group was 21.6 kg/m^2. 18.4% of study cases had severe stenosis compared to 16.8% of control cases. 17.5% of decedents with a BMI ≤ 55 had severe stenosis compared to 11% of decedents with BMI > 55. Severe stenosis was not identified in any decedent with a BMI > 75.

Conclusions: There is no statistically significant difference in the prevalence of severe CAA between morbidly obese cases and control cases. Data suggests that those with a BMI > 75 die from causes other than CAA, and that those with a BMI > 55 have less severe CAA than those with a BMI < 55.

373 Elevated Myocardial Expression of Heterogeneous Nuclear Ribonucleoprotein C Predicts Recovery in Patients with Acute Systolic Heart Failure

JR Stone, MJ Semigran, KA Parks. Massachusetts General Hospital, Boston, MA.

Background: Acute nonischemic systolic heart failure (NISHF) is a major cause of morbidity and mortality. Predicting which patients will recover from NISHF and which need advanced therapies is a significant challenge. We hypothesized that the level of expression of heterogeneous nuclear ribonucleoprotein C (hnRNP-C) in cardiac myocytes might be helpful in predicting recovery of cardiac function in patients presenting with new-onset systolic heart failure.

Design: The study group consisted of 8 patients who presented with NISHF and underwent endomyocardial biopsy, which was negative for myocarditis. The endomyocardial biopsies were stained for hnRNP-C, and the percentage of positively staining myocytes was correlated with recovery of left ventricular ejection fraction (LVEF) assessed by echocardiography. Three normal control hearts from autopsies were also stained for hnRNP-C.

Results: By 17 months follow-up, 5 patients demonstrated "recovery" defined as an improved LVEF (baseline 0.20 ± 0.03 (mean ± SD), follow-up 0.43 ± 0.12, P<0.01) and 3 patients did not have significant improvement "no recovery" in LVEF (baseline 0.17 ± 0.07, follow-up 0.26 ± 0.01). The mean ages were 44 ± 14 years for the recovery group, 41 ± 16 years for the no recovery group, and 51 ± 8 years for the controls. There was no significant difference in initial LVEF between the two heart failure groups (0.20 ± 0.03 vs 0.17 ± 0.07 P=0.4). All patients were on an optimal heart failure medical regimen. Patients in the recovery group had significant upregulation of hnRNP-C on initial biopsy (65±11% of myocytes) compared with the no recovery group (34±9%) and compared with control hearts from autopsies (31±4%) (P<0.003).

Conclusions: Our results suggest that the level of expression of hnRNP-C in cardiac myocytes in patients with acute NISHF may be predictive of short-term recovery of LVEF. This may have clinical implications in the decision to offer advanced therapies to NISHF patients. Further evaluation of the utility of hnRNP-C as a prognostic marker in a larger population of patients with heart failure is necessary.

374 The Phospholamban p.Arg14del Mutation-Related Cardiomyopathy Is an Arrhythmogenic Cardiomyopathy and Protein Aggregation Disease

WP te Rijdt, P van der Zwaag, MP van den Berg, P van Tintelen, AJ Suurmeijer. Pathology, Cardiology and Genetics, Groningen, Netherlands.

Background: In a Dutch cohort, the nondesmosomal phospholamban (PLN) p.Arg14del mutation was recently identified in 13% of patients clinically diagnosed with idiopathic dilated cardiomyopathy (DCM) and 12% of patients diagnosed with arrhythmogenic right ventricular cardiomyopathy (ARVC). We characterized the gross and microscopic pathologic features of 16 complete heart specimens from patients carrying this heterozygous p.Arg14del PLN mutation. In addition, we hypothesized that the p.Arg14del mutation leads to aggregation and autophagocytosis of mutant PLN protein in cardiomyocytes.

Design: The 16 hearts studied were from 8 male and 8 female patients with a mean age of 46 years (range 22-71 years). Eleven hearts were from autopsies and 5 were explants. Six (6/11) autopsy cases were from patients with sudden unexpected death. The other 10 patients were clinically evaluated by widely accepted task force criteria for ARVC and DCM. IHC for PLN was performed to visualize protein aggregation. IHC for sequestosome-1 (SQSTM-1/p62) was applied to visualize autophagocytosis. Double IHC staining was performed to study co-localization of SQTSM-1 and PLN in aggresomes.

Results: By pathologic examination, all 16 hearts showed a predominant ARVC morphologic phenotype with gross (9/16) or microscopic (7/16) fibrofatty replacement of the RV wall. LV involvement was characterized by extensive transmural (12/16) or epicardial (4/16) interstitial fibrosis and myocyte hypertrophy. In 8/16 hearts microscopic fibrofatty change was present in the LV, and this was most pronounced in the posterolateral and anterolateral wall. By clinical analysis, all 10 patients had left ventricular dysfunction (low LV ejection fraction and fractional shortening) and 6 patients had a dilated left ventricle. Using task force criteria 4/10 were diagnosed with combined ARVC/DCM, 2 with DCM, and 1 with ARVC. With IHC, large perinuclear PLN protein aggregates were present in cardiomyocytes in both the RV and LV myocardium in all 11 hearts included. The mean number of PLN aggregates was 8 per 5 mm^2 (range 2-19) in RV myocardium and 14 per 5 mm^2 (range 2-39) in LV myocardium. Co-localization of SQTSM-1 and PLN was observed in some of these aggregates.

Conclusions: Our series of 16 hearts revealed that the PLN p.Arg14del mutation-related cardiomyopathy is a biventricular cardiomyopathy, showing a combination of features of ARVC and (developing) DCM. Moreover, this PLN cardiomyopathy is a cardiac proteinopathy, characterized by perinuclear PLN aggregates that are degraded by autophagy.

375 Pathology of Stentless Bioprosthetic Valves: Mode and Cause of Failure

M Valente, M Della Barbera, C Basso, G Thiene. University of Padova, Medical School, Padova, Italy.

Background: Stentless valves have represented an important step forward in the history of surgery of valve disease. Lack of prosthetic prongs minimizes transvalvular gradient and favours regression of left ventricular hypertrophy. The disadvantage consists of the time consuming suturing, requiring surgeon training and skill. Both glutaraldehyde fixed porcine and pericardial stentless bioprostheses (BPs) have been conceived and introduced in the clinical setting. While structural valve deterioration (SVD) in stented porcine and pericardial BPs has been extremely investigated, scarce information on stentless BPs is available.

Design: We reviewed the pathology of 70 stentless BP several models, either porcine (Toronto S. Jude Medical, Cryolife, BioCor, Prima Plus Carpentier-Edwards) or pericardial (Freedom Stentless Sorin). All but two were implanted in aortic position. By excluding cases with secondary failure (leak, endocarditis), we focused on the 34 stentless BPs which failed because of SVD.

Results: Thirty six BPs failed because of histologically proven endocarditis or because of paravalvular leak and were excluded from the study. In the remaining 34 the leading cause of SVD was dystrophic calcification at the commissures or primary tears with cusp tearing, and the mode of failure was incompetence frequently so abrupt as to require urgently redo. Lipidosis was observed at histology and concurred to tissue degeneration (Figure 1).

Stentless BPs: cause and mode of SVD

Stentless BP model	Nr	Mean patient age (yrs)	Time in place (mos)	Major pathology	Dysfunction
Toronto S. Jude Medical	10	46.9±9.98	119.1±25.08	Calcific dystrophy, commissural tearing, lipidosis, fibrous pannus, primary tearing	INCOMPETENCE
Cryolife	11	62.09±14.90	113.09±33.22	Calcific dystrophy, commissural tearing, lipidosis, perforations	INCOMPETENCE
BioCor	5	67.2±5.44	113.8±35.20	Calcific dystrophy, commissural tearing, primary tearing	INCOMPETENCE STENOINCOMPETENCE
Freedom Stentless Sorin	6	65.66 ±13.58	76.83±14.49	Calcific dystrophy, commissural tearing, lipidosis	INCOMPETENCE STENOSIS
Prima Plus Carpentier-Edwards	2	65.5±6.36	134±65.05	Calcific dystrophy, commissural tearing, lipidosis	INCOMPETENCE

Figure 1

Conclusions: Dystrophic calcification, lipid insudation, with cusp tearing and incompetence are the substrate and mode of failure of stentless BPs. Longest durability was observed in stentless valves with anticalcification treatment . Surgical pathology is in keeping with a redo by valve-in-valve TAVI.

376 Temporal Small Arterial Inflammation Is Common in Patients with Giant Cell Arteritis

CL Zhao, A Amin. Rhode Island Hospital, Providence, RI.

Background: Giant Cell Arteritis (GCA) is considered a systemic arteritis mainly involving medium to large arteries. There is little information about arteriolar arteritis in GCA with unknown implications.

Design: Between 2008 and 2013, 90 temporal artery specimens were found in the archives of Rhode Island Hospital. The slides and medical records were reviewed retrospectively, comparing the manifestations and clinical correlates. The following parameters were reviewed: age, gender, fever, headache, scalp tenderness, jaw claudication, visual symptom (diplopia, blurred vision and diminished acuity), weight loss, ESR, hemoglobin, p-ANCA, ANA, and polymyalgia rheumatica. Statistical analysis was performed utilizing SigmaStat software, version 3.5 for Man-Witney Rank-Sum test and Fisher Exact test. $P<0.05$ was considered as statistically significant.

Results: Sixty-two patients met the 1990 American College of Rheumatology (ACR) criteria for the diagnosis of GCA and were included in the analysis [sex distribution: 16 males and 46 females (p=0.477); age range 51-90 years (mean of 76.5±1.067)]. Twenty-six specimens (5 male, 21 female) demonstrated temporal arteritis and small arterial inflammation (TSAI) and 36 specimens (11 male and 25 female) demonstrating temporal arteritis without small arterial inflammation (T-non-SAI). Binary logistic regression was applied with the attributes found to be significantly related with TSAI; however there was no statistical difference in signs and symptoms and hemoglobin level between the TSAI and T-non-SAI groups. ESR was 80 mm/hour in TSAI and 62 mm/hour in T-non-SAI; p=0.095). Serum p-ANCA was assessed in 12 patients and 2 patients were positive (≥1:20). Both cases showed severe clinical manifestation of temporal arteritis including polymyalgia rheumatica and vision loss that required Emergency Room admission and high-dose steroids.

Conclusions: Simultaneous involvement of arterioles and medium to large sized arteries is common in GCA. Despite a postulation for coexisting microscopic polyangiitis and GCA, the disease manifestations and course is similar between TSAI and T-non-SAI cases in our series. We believe that in the context of GCA, involvement of smaller arteries should be expected. TSAI with p-ANCA positive may have more severe symptoms and require aggressive therapy.

Cytopathology

377 Immunoisolation of Pancreatic Epithelial Cells from EUS-FNA with Magnetic Beads for Downstream Molecular Application

A Afify, S Urayama. UC Davis, Sacramento, CA.

Background: Evaluation of pancreatic masses is routinely performed by endoscopic ultrasound-guided fine needle aspiration (EUS-FNA). However, molecular analyses of the tumor cells in FNA samples are limited by the significant cellular heterogeneity. The goal of the current study is to evaluate a magnetic immunoconcentration technique for isolating pancreatic epithelial cells from needle aspirates and to demonstrate that the isolated cells could be utilized for molecular analysis.

Design: All samples included in the study were obtained by EUS-FNA. After adequate sampling for cytopathological evaluation, three additional needle passes were collected individually into a microfuge tube with RNA*later* and stored at –80ºC. Based on the final cytopathological diagnosis, 17 adenocarcinoma, 2 lymphoma, and 2 benign cases were retrieved from the collection for further analyses. After thawing the frozen specimen, a cytospun slide was prepared and stained with Pap stain for cytology evaluation to confirm the diagnosis and determine the types of cells present. Epithelial cells were isolated using anti-human epithelial cell specific antibody-bound magnetic beads (Invitrogen, Carlsbad, CA). The isolated cellular component was examined cytologically and Genomic DNA was extracted, quantitated and evaluated with methylation-specific PCR for methylation of the promoter region of the cyclin D2 gene.

Results: Evaluation of cytospun slides prepared directly after thawing the frozen specimen confirmed the original diagnosis and the presence of the neoplastic cells admixed with histiocytes, lymphocytes, fibro-connective tissue, and RBCs. After optimization of the technique, we isolated malignant epithelial cells successfully from all adenocarcinoma cases. Normal pancreatic ductal cells were isolated from the 2 benign cases. No cells could be isolated from the cases of lymphoma. The mean DNA yields was 357 ng. Methylation-specific PCR for cyclin D2 showed a methylated state at the promoter region, demonstrating feasible evaluation of the methylation status.

Conclusions: Magnetic immunoconcentration of pancreatic EUS-FNA specimens, as described in this study, is a practical method of isolating pancreatic epithelial cells from needle aspirates. This methodology is a relatively easy allowing molecular analysis of pancreatic neoplasms, which may be adaptable for future molecular signal or biomarker assays.

378 Proteomic Analysis and Characterization of Effusion Fluid

A Afify, A Eldridge, B Chromy. UC Davis, Sacramento, CA.

Background: Tumor cells in malignant effusion shed surface proteins and secrete growth factors and cytokines, which leads to changes in the proteome of effusions. Expression pattern analysis of these proteins could be used to differentiate malignant from benign effusions and provide potential diagnostic biomarkers. The purpose of this study was to compare the expression profiles of fractionated proteins from benign and malignant effusions in order to detect and identify proteins that show differential expression.

Design: Effusion samples were centrifuged and the supernatant was retained and stored at -80°C. Removal of six high abundant proteins was performed using affinity chromatography. The remaining portion of each sample was individually labeled with fluorescent dyes and proteins were separated using two-dimensional differential gel electrophoresis technique. The gels were scanned using specific excitation/emission wavelengths for each dye using a Typhoon 9410 scanner. Image analysis was performed using Amersham DeCyder 7.0 software for spot detection, quantitation and gel-to-gel matching. Differential expression of proteins between benign and malignant effusions was determined based on set of selection criteria include t-test score, average ratio and one-way ANOVA. Selected gel spots were subjected to protein identification by liquid chromatography-tandem mass spectrometry. Peak lists were generated for each protein spot and searched against the human International Protein Index database using Mascot search engine.

Results: We analyzed 28 effusion samples including 12 malignant (breast, lung and ovary, 4 cases each) and 16 benign. The mean number of protein gel spots identified among all cases was 1400 ± 200.Thirty five protein spots showing differential protein expression levels between benign and malignant effusions were further evaluated using principle component analysis and hierarchical clustering. Malignant effusions showed 19 up-regulated and 16 down-regulated protein spots. Of the 35 differential protein spots, 24 were successfully identified and was subjected to functional analysis and correlated to the cause of the effusion.

Conclusions: Our results represent a first step toward understanding the complexity of effusion proteomes. This work provides a baseline expression profile for future use in determining key proteins that can differentiate between benign and malignant effusions. We expect that this work will ultimately contribute to improved biomarker discovery. In addition, proteins that change in expression may lead to additional clues to help our understanding of cancer.

379 EUS-FNA of Focal Liver Lesions: A Retrospective Study from an Academic Tertiary Center

R Albadine, G Soucy, B Nguyen, S Paquin, A Sahai, G Gariepy. Centre Hospitalier de l'Université de Montréal, Montreal, QC, Canada.

Background: EUS-FNA of the liver is a safe procedure with high diagnostic yield and impact on patient management (Evidence level 2+ according to European Society of Gastrointestinal Endoscopy). Only a few studies with large cohort were identified in the literature. We report our experience of EUS-FNA cytology of focal liver lesions.

Design: All liver lesions with EUS-FNA, performed by 2 gastroenterologists, between 2003 to 07-2013 were retrieved in our lab. All available data were collected. Rapid on site cytopathology evaluation (ROSE) was available for almost all cases. Immunohistochemistry (IHC) study was performed when cell block was available. Cases were classified as inadequate (acellular, non-representative), negative for malignant cells (adequate and benign), atypical, suspicious and positive for malignant cells.

Results: We identified 593 EUS-FNA specimens. Of these, 429 were positive, 130 were negative, 12 were atypical, 5 suspicious and 17 (2%) were non diagnostic. There were 403 carcinomas included:313 adenocarcinomas (cholangio and metastatic), 2 squamous cell carcinomas, 27 neureodocrine tumors, 25 small cell carcinomas (SCC), 26 non SCCs and 9 hepatocellular carcinomas (HCC). A precise diagnosis was possible in 9 of the 26 other positive cases: 3 gastrointestinal stromal tumors; 5 Lymphomas: 4 non-Hodgkin lymphomas and 1 Lymphocyte-depleted classical Hodgkin lymphoma; and 1 Melanoma. The benign lesions were 10 abscesses, 2 granulomas and 2 with steatosic hepatocytes. Of the 5 cases with suspicious cytology: 2 patients were submitted to biopsy and the diagnosis was HCC in one case and metastatic mucinous adenocarcinoma, in the other. Most atypical cytology diagnosis was post-radiation. Discrepancies were seen in 3 cases of HCCs: one HCC with lipidic changes was misdiagnosis as steatosis, and 2 well differentiated HCC, where cytologic diagnosis was on smears only without cell block for IHC. EUS-FNA was repeated in 13 patients with inadequate, negative or atypical cytology. Four were reclassified as positive.